buildings

MDPI

Article

Asphalt Layer Cracking Behavior and Thickness Control of Continuously Reinforced Concrete and Asphalt Concrete Composite Pavement

Sheng Li [1], Yu Sun [1], Lukai Xu [1], Shiqing Yu [1,*], Xiaodong Liang [2] and Ji Ye [3]

[1] Key Laboratory of Special Environment Road Engineering of Hunan Province, Changsha University of Science & Technology, Changsha 410114, China; lishengttt@csust.edu.cn (S.L.); 164798189@stu.csust.edu.cn (Y.S.); xulukaiii@163.com (L.X.)
[2] Hunan Lianzhi Technology Co., Ltd., Changsha 410019, China; longyw9@163.com
[3] School of Materials Science and Engineering, Central South University, Changsha 410017, China; sy164798189@163.com
* Correspondence: shiqingyuu@stu.csust.edu.cn; Tel.: +86-15673121008

Abstract: Based on thermal–mechanical coupling simulation analysis and physical engineering tracking observation, the mechanical behavior and response of a continuously reinforced concrete and asphalt concrete (CRC + AC) composite pavement layer were analyzed, and the causes of cracking on the surface and bottom of the asphalt layer were revealed. Studies have shown that under normal driving conditions, the AC layer, which is usually in the position of the wheel load gap and wheel load side, more easily generates a longitudinal "corresponding crack". Compared to normal driving, longitudinal cracks are generated more easily inside of the curve, and transverse cracks occur more easily on poor stadia curves. When the AC layer thickness is less than 8 cm, the AC layer is more prone to bottom-up cracking, and it is more prone to top-down cracking when it is more than 8 cm thick. Comprehensively considering the tensile stress, shear stress, and the thickness of the AC layer, it is recommended that the suitable thickness range of the AC layer is 8 cm~14 cm. The calculated results show good agreement with the physical engineering investigation. The research results can provide a theoretical and scientific basis for cracking control and the rational design of a CRC + AC composite pavement layer.

Keywords: road engineering; composite pavement; numerical simulation; thermal–mechanical coupling; cracking behavior

Citation: Li, S.; Sun, Y.; Xu, L.; Yu, S.; Liang, X.; Ye, J. Asphalt Layer Cracking Behavior and Thickness Control of Continuously Reinforced Concrete and Asphalt Concrete Composite Pavement. *Buildings* **2022**, *12*, 1138. https://doi.org/10.3390/buildings12081138

Received: 8 July 2022
Accepted: 28 July 2022
Published: 1 August 2022

Publisher's Note: MDPI stays neutral with regard to jurisdictional claims in published maps and institutional affiliations.

1. Introduction

CRC + AC composite pavement is a kind of pavement structure that includes an AC layer on top of a continuously reinforced concrete (CRC) slab. This kind of pavement structure is one of the main structural forms of long-life pavement for heavy-duty traffic in China. It has a high bearing capacity, good driving comfort, and low maintenance and repair costs. CRC + AC composite pavement is a kind of rigid base asphalt pavement. The horizontal strain at the bottom of the asphalt layer is lower due to the modulus dependency of the pavement base [1], which means that rigid base asphalt pavement has a longer fatigue life. However, owing to the thinness AC layer of CRC + AC, once cracks occur, they easily expand throughout the entire AC layer. Using physical engineering tracking observation, cracks in the AC layer were found to be major problems of CRC + AC composite pavement. As a type of durable pavement with a high initial investment cost, the cracking behavior of the AC layer, if not effectively controlled, increases maintenance costs, affects the service life of the asphalt layer, and even has an impact on the durability of CRC slabs, resulting in wasted investments.

Since it is difficult to study the pavement structure problem with a full-scale test, most of the existing studies have been conducted using simulation. Finite element analysis and discrete element analysis are the two most commonly used research methods. Liu and Zhang [2] applied the finite element method to analyze the pavement response to different vehicular speeds and pavement roughness, and the simulation results were in good agreement with the measured data. Shen et al. [3] found that the semi-analytical finite element method was more efficient when analyzing pavement responses induced by moving vehicles. Ban et al. [4] studied the performance and damage characteristics of composite pavement through laboratory tests incorporated with mechanistic finite element modeling. Ling et al. [5] used a finite element model to study the thermal cracking fatigue life of asphalt pavement. Yong et al. [6] used a three-dimensional discrete element model embedded with a temperature gradient and fatigue damage to investigate the mechanical response of asphalt surfaces under moving traffic loads. The results indicated that the model could be used to predict the mechanical response of asphalt surfaces under repeated loads. In order to more accurately simulate the action of the wheels on the road surface, some research has been carried out in this area. Chen and Zhang [7] developed a tire–pavement finite element model to study the influence of different indexes on the dynamic behavior of flexible pavement, and the model was validated by a field test. Lu et al. [8] compared the mechanical response of an asphalt mixture under homogeneous loads to that under inhomogeneous loads, and the average stresses on the interior were significantly different. The finite element method is already a well-established method for the study of pavement structures.

The accurate simulation of tire loads facilitates the study of top-down cracking mechanisms. Severe top-down cracking in asphalt pavements has recently piqued the interest of the engineering community [9]. Ziari et al. [10] used finite element models to determine the effects of vehicle position, thickness, and stiffness of layers on the fatigue life of pavements. The results show that top-down cracking was easier to develop when the wheels were symmetrically located relative to the crack plane, and the surface layer's stiffness had the most effect on the fatigue life of the pavement. Islam and Tarefder [11] developed a closed-form equation to calculate damage due to repeated day–night temperature fluctuations. The top-down longitudinal cracking was predicted by this closed-form equation, and the results show that the top-down longitudinal cracking prediction error decreased by 13% when combining the temperature-induced damage with the traffic-induced damage. Wu and Muhunthan [12] predicted top-down cracking through a mechanistic–empirical model, and suggested adopting an asphalt mix with a relatively higher horizontal failure strain value to reduce top-down cracking. Aliha et al. [13] investigated the influence of different indexes on the fracture parameters using the finite element method. The results showed that a stiffer aggregate or a softer fine aggregate matrix part in the top-down cracking tip can slow crack expansion. Rith et al. [14] studied the influence of design parameters, such as thickness and stiffness, on asphalt layer cracking behavior under thermal loading; the results showed that top-down cracking appeared when the slab base had a low elastic modulus. Tajdini and Taherkhani [15] described the effects of the crack type, position, and length, as well as vehicle tire inflation pressure and axle load on the performance of cracked asphalt pavement. For semi-rigid base asphalt pavement, in general, top-down cracking results in higher mechanical responses than bottom-up cracking. Zhao et al. [16] investigated the mechanism of top-down cracking based on the horizontal tensile strain; the results indicated that the occurrence of top-down cracking increased with an increased temperature and asphalt content. The problem of top-down cracking is also a serious problem for CRC + AC composite pavements, but few studies have been conducted on it.

CRC + AC composite pavements always have a thicker AC layer because of the high load-bearing capacity of the CRC layer. However, considering the protection of the CRC layer, the asphalt layer should not be too thin. There are numerous studies showing the importance of a reasonable thickness of the asphalt layers. Shabbir Hossain et al. [17] investigated the thermal behavior and performance in the first 4 years after opening two westbound lanes of US 60 to traffic in Henrico County. The results indicated that the asphalt overlayer reduced the temperature gradient within the CRC layer. Fardin and

Santos [18] evaluated the effects of pavement design variables on fatigue cracking and rutting resistance, and asphalt layer thickness had the biggest impact on reducing damage. Xie and Wang [19] analyzed the effect of thermal cycles on reflective cracking in composite pavement; the results showed that a thicker asphalt overlayer significantly decreased the reflective cracking potential at the crack initiation phase. Alae et al. [20] studied the fracture mechanisms behind top-down crack propagation and investigated the fatigue life of pavements under dual tire loads using finite element analysis. The stress intensity factor (SIF) calculation results indicated that it is necessary to consider the temperature gradient in the asphalt concrete layer to determine the critical SIF, and the top-down crack growth rate significantly depends upon the AC thickness and the base layer type. Diallo and Akpinar [21] assessed the mechanical behaviors of an asphalt concrete overlaid on a jointed plain concrete pavement under traffic loading; the results showed that asphalt concrete thickness had the biggest influence on the pavement response. However, studies on the reasonable thickness of a CRC + AC composite pavement layer are rare.

Therefore, in this study, a thermal–mechanical coupled finite element model was used to reveal the mechanical behavior and top-down crack generation mechanism. The reasonable thickness of the AC layer was determined by analyzing the shear stress and longitudinal tensile stress, and the analysis results were compared with those of physical engineering observations.

2. Simulation Methods

2.1. Pavement Structure and Parameters

To study the mechanical behavior of a CRC + AC pavement layer, a thermal–mechanical coupling CRC + AC pavement model was established. The pavement structure and basic material mechanical parameters under different temperatures [22,23] are shown in Table 1. F16 mm ribbed rebar was used for the longitudinal steel of the CRC layer, and F12 mm ribbed rebar was used for the transversal steel. The longitudinal and transversal reinforcement ratios were 0.6% and 0.1%, respectively. The modulus of the ribbed rebar was 2.0×10^5 MPa, and the density was 7800 kg·m^{-3}. Both the longitudinal and transversal steel were set in the intermediate position of the CRC layer and embedded into the layer in the form of continuous steel mesh using the embedded region constraint type in ABAQUS. There were transverse cracks set in the CRC layer, the crack spacing was 1.5 m, and the width was 0.5 mm, using virtual filler to simulate the load transfer of the crack. The thermo-physical parameters required to calculate the temperature field are detailed in reference [23]. To clearly show the research process, the research flow chart is shown in Figure 1.

Table 1. Material parameters of structural layers.

Structural Layer	Thickness (m)	Elastic Modulus /MPa					Poisson's Ratio	Damping Ratio	Density (kg·m^{-3})
		−30 °C	−20 °C	−10 °C	0 °C	20 °C			
AC	0.08	14,000	9000	4500	1400	870	0.300	0.90	2300
CRC	0.24			29,000			0.167	0.80	2400
Cement-treated base (CTB)	0.40			2000			0.250	0.80	2200
Soil subgrade	–			60			0.400	0.40	1800

2.2. Establishment of Thermal–Mechanical Coupling Load Model

A sequential coupling method was used to achieve the coupling of the temperature and vehicle loads. The implementation in ABAQUS was performed by adding the calculated temperature field data to the predefined field module and, at the same time, adding a pressure load.

To calculate the temperature field, the user-defined subroutine FILM in the load module of ABAQUS was used to achieve the heat exchange of the pavement surface and the air, and the user-defined subroutine DFLUX in the interaction module was used to simulate the effect of solar radiation. The on-site measured air temperatures used to achieve the temperature and convective exchange are shown in Table 2, and the index used to simulate solar radiation is shown in Table 3. The initial temperature of the pavement structure was set to 0 °C, and the thermophysical parameters are shown in Table 4. The temperature field of the pavement structure was obtained using transient and steady-state heat transfer analysis. The action was repeated with the set solar radiation and air temperature data, and the final stable temperature field of the pavement structure was taken as the calculation result (5 cycles). The temperature field calculation logic is shown in Figure 2. According to a previous study and article [24], the pavement bears higher tensile stress at 6:00 am. So, the calculated 6:00 am pavement structure temperature field was imported in ABAQUS as an unfavorable temperature condition.

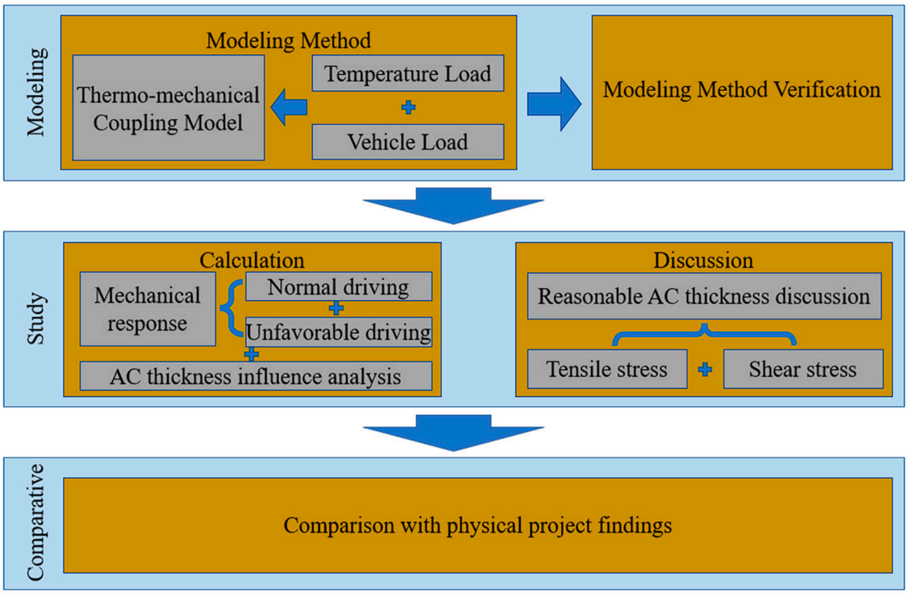

Figure 1. Research process diagram.

Table 2. Measured air temperatures of 24 hours in cold seasons in a region (°C).

Time	Temperature	Time	Temperature	Time	Temperature	Time	Temperature
0:30	−2.06	6:30	−7.58	12:30	2.93	18:30	2.83
1:00	−2.56	7:00	−6.59	13:00	2.87	19:00	3.19
1:30	−1.65	7:30	−8.64	13:30	3.22	19:30	2.62
2:00	−2.05	8:00	−6.87	14:00	4.40	20:00	2.41
2:30	−2.99	8:30	−5.46	14:30	4.23	20:30	1.98
3:00	−5.39	9:00	−4.61	15:00	4.98	21:00	1.63
3:30	−3.84	9:30	−2.52	15:30	4.99	21:30	1.40
4:00	−4.65	10:00	−1.67	16:00	4.94	22:00	0.80
4:30	−6.82	10:30	−0.84	16:30	4.87	22:30	0.16
5:00	−6.37	11:00	2.28	17:00	4.55	23:00	−0.27
5:30	−5.21	11:30	2.90	17:30	3.63	23:30	−1.08
6:00	−6.84	12:00	2.56	18:00	2.99	24:00	−1.70

Table 3. Parameters needed to simulate solar radiation.

Maximum Air Temperature (°C)	Lowest Air Temperature (°C)	Total Solar Radiation Q (MJ/m^2)	Daylight Hours c (h)	Average Daily Wind Speed v (m/s)
4.99	−8.64	9.14	6.5	2.9

Table 4. Thermophysical parameters of pavement materials.

Parameters		AC	CRC	CTB	Soil Subgrade
Thermal conductance/(J·(m·h·°C)$^{-1}$)		4670	6200	5620	5620
Heat capacity/(J·(kg·°C)$^{-1}$)		924	780	911	1040
Temperature shrinkage coefficient (10^{-5}/°C)	10 °C	3.5	1	0.98	0.45
	0 °C	4.3			
	−10 °C	3.8			

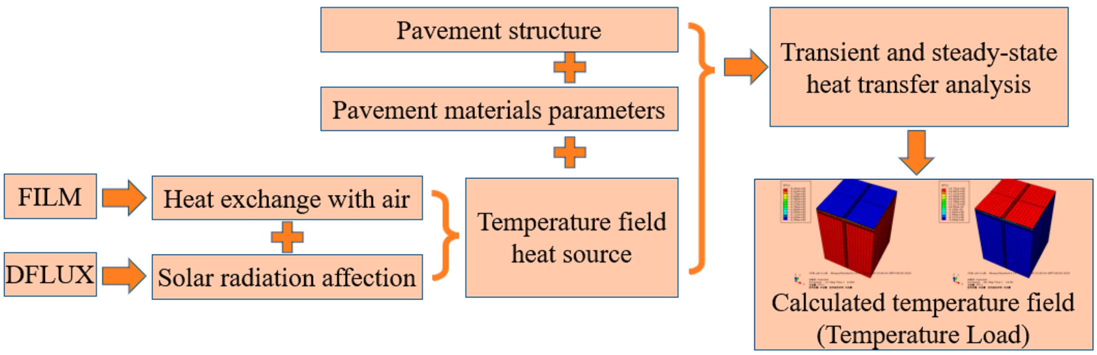

Figure 2. Research process diagram.

A 100 kN two-wheel axle load was applied as the vehicle load, and a single wheel was simplified as a three-dimensional non-uniform semi-sinusoidal load, as shown in Figure 3 [25–28]. P_i (i = 1, 2, 3) was the compressive stress on each wheel path that ran parallel to the normal direction of the pavement. q_i (i = 1, 2, 3) was the transverse horizontal force perpendicular to the normal direction of the road, and f_i (i=1, 2, 3) was the frictional force opposite to the driving direction on each wheel path.

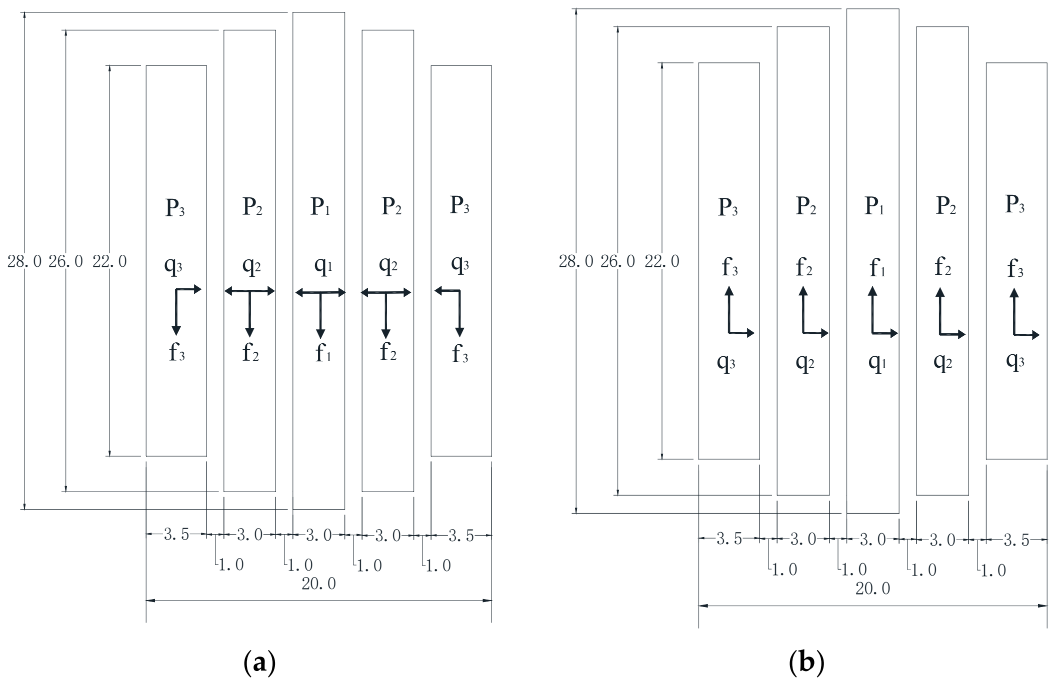

Figure 3. Three-dimensional non-uniform load (size unit is cm): (**a**) normal driving; (**b**) unfavorable driving.

Under normal driving, according to the paper by [8], the distribution of the pressure values (P_1, P_2, P_3), transverse force (q_1, q_2, q_3), and frictional force (f_1, f_2, f_3) on the tread is shown in Table 5. Emergency braking in high-speed driving was considered an unfavorable working condition of the pavement structure. The transverse forces were determined using Formula (1), and the frictional forces were determined using Formula (2) [23].

$$q = Pv^2/rg \tag{1}$$

where q represents the transverse force, MPa; v represents the speed of the vehicle, m/s; r represents the radius of curve, m; g represents the acceleration of gravity, 9.8 m/s^2.

$$f = \alpha \cdot P \tag{2}$$

where f represents the frictional force, MPa; α, represents the frictional force coefficient; P represents the pressure values, MPa.

According to the above equations, the transverse force was determined by the driving speed and curve radius of the route. The driving speed was determined to be 27.78 m/s (100 km/h), the radius of the curve was determined to be 450m, and the acceleration of gravity was 9.8 m/s^2. The frictional force coefficient in emergency braking was 0.5 [23], and the calculated P_i (i = 1, 2, 3), q_i (i = 1, 2, 3) and f_i (i = 1, 2, 3) are shown in Table 5.

Table 5. Value of tire grounding pressure and surface stress (MPa).

Driving Status	P_1	P_2	P_3	q_1	q_2	q_3	f_1	f_2	f_3
Normal driving	0.870	0.680	0.460	0.157	0.122	0.810	0.174	0.136	0.900
Unfavorable driving	0.870	0.680	0.460	0.157	0.122	0.810	0.435	0.340	0.230

2.3. Verification of Simulation Method

The reliability of the thermal–mechanical coupling simulation method was verified using a set of surface deflection basin data tested on a highway with a CRC + AC pavement structure in Hunan Province, China with a falling weight deflectometer (FWD).

A finite element model with the same pavement structure as the highway was established, and a half-sine wave load with a peak value of 0.714 MPa, an action radius of 15 cm, and an action time of 30 ms was applied to simulate the FWD load. The deflection value at the same temperature as that measured by the physical engineering study was calculated. The comparison between the FWD measured deflection and the calculated deflection is shown in Figure 4.

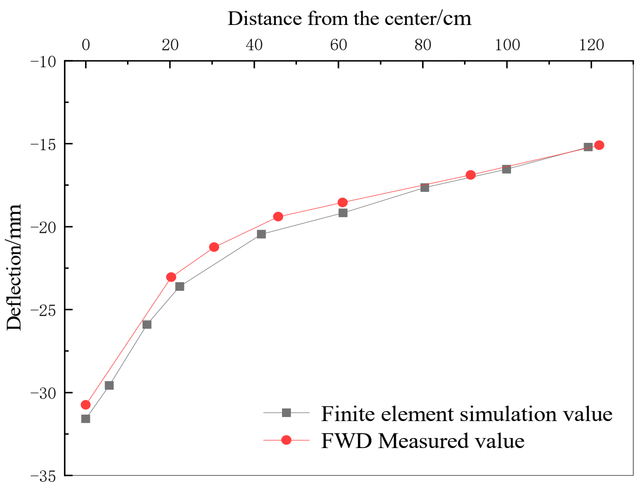

Figure 4. Comparison of calculated and FWD-measured deflection values.

As shown in Figure 4, the maximum error between the calculation results and the measured deflection value was 6.3%. This indicates that the modeling method of the thermal–mechanical coupling calculation model of CRC + AC composite pavement is reasonable and reliable and can be used to simulate the mechanical behavior of CRC + AC composite pavement structure.

2.4. Calculation Position Description

The CRC + AC composite pavement structure is complex, and the mechanical response of the pavement structure is different from that of semi-rigid base and flexible base asphalt pavement under the coupling action of temperature and a three-dimensional non-uniform distributed dynamic load. It is even different from that of the traditional rigid base asphalt pavement. The mechanical behavior analysis of the AC layer of the CRC + AC composite pavement structure has theoretical significance for the investigation of the cracking inducement of the AC layer.

The longitudinal and transverse tensile stress and shear stress of the AC layer along the CRC layer cracks were slightly higher. To explain this phenomenon, a mechanical response analysis was conducted on the AC layer section along the micro-crack of the CRC layer perpendicular to the direction of travel. A schematic of the calculation points is shown in Figure 5.

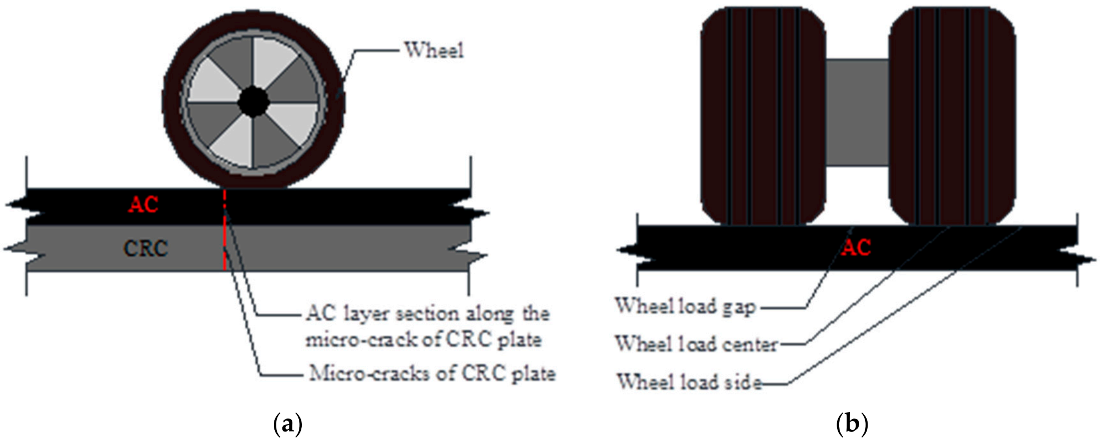

Figure 5. Schematic of calculation points: (**a**) AC layer section; (**b**) calculation points.

3. Results and Discussion

The asphalt surface layer of the CRC + AC composite pavement was thin, and cracks were more likely to penetrate the entire asphalt surface layer. Rainwater entering the pavement through cracks caused an increase in the transverse crack width, reinforcing corrosion and the void beneath the slab, which affected the durability of the CRC layer. In order to control the cracking of the AC layer and enhance the durability of the CRC + AC composite pavement, it was necessary to determine the reasonable thickness of the asphalt surface.

3.1. AC Layer Mechanical Behavior Analysis

3.1.1. Normal Driving

The stresses in the AC layer above the micro-cracks of the CRC layer under the coupled action of a wheel load and temperature in normal driving conditions were calculated and analyzed. The distribution of stress is shown in Figure 6a–c.

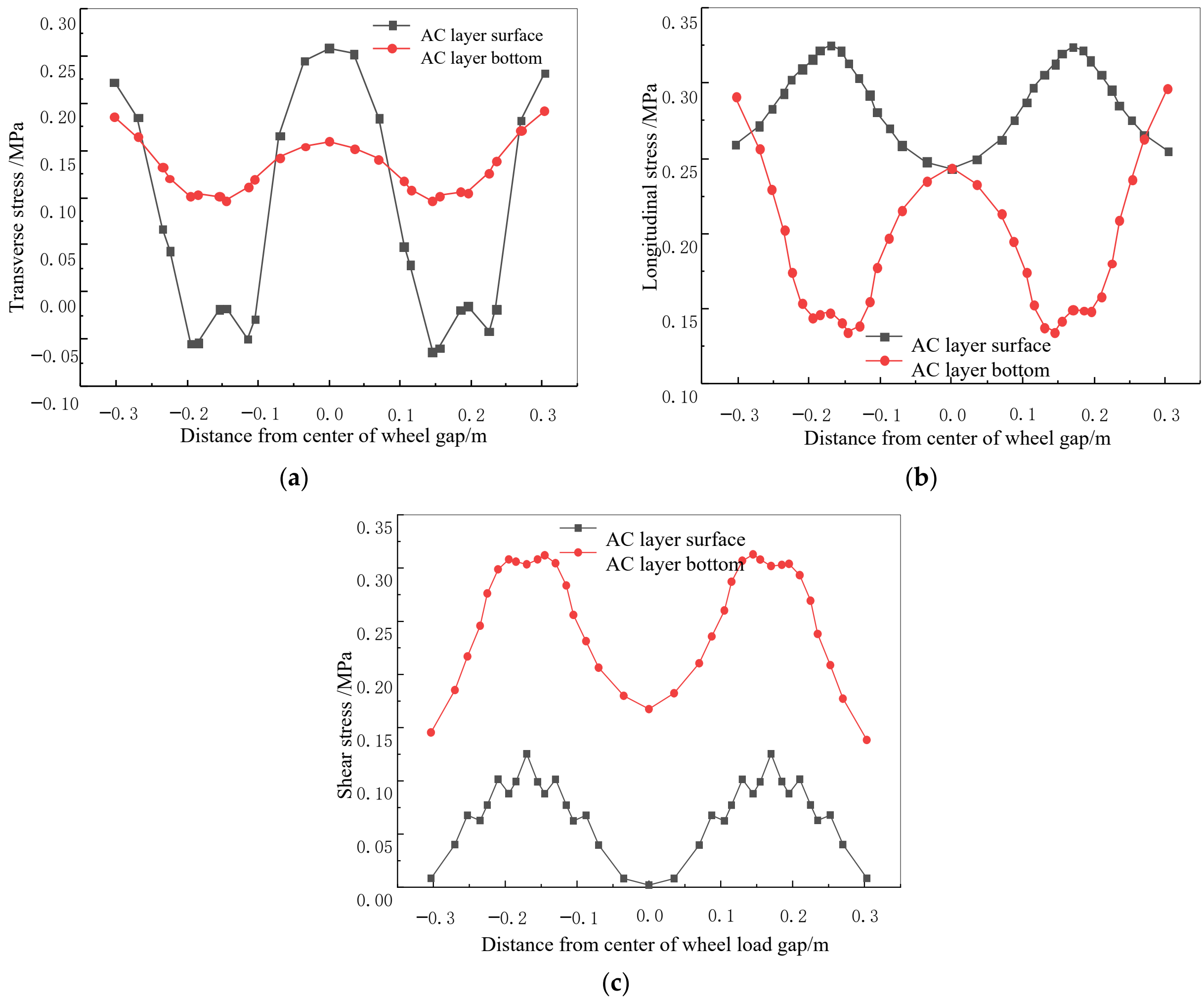

Figure 6. Stress of AC layer under normal driving conditions: (**a**) distribution of transverse stress; (**b**) distribution of longitudinal stress; (**c**) distribution of shear stress.

As shown in Figure 6a, both the wheel load side and the wheel load gap suffered greater transverse tensile stress on the surface and bottom of the AC layer under the thermal–mechanical coupling load. Compared to the surface and bottom of the AC layer, only the transverse tensile stress at the bottom of the AC layer at the wheel load center was higher across the entire wheel load range. The greatest transverse tensile stress values were 0.260 MPa at the wheel load gap, 0.138 MPa at the wheel load center, and 0.233 MPa at the wheel load side. It can be seen in Figure 6b that the longitudinal tensile stress was higher at the wheel load side of the AC layer bottom and the wheel load center of the AC layer surface, and the greatest longitudinal tensile stress values at each position were 0.297 MPa and 0.324 MPa. The longitudinal tensile stress almost achieved the same value of 0.243 MPa at the wheel load gap. In Figure 6c, it is clearly demonstrated that the shear stress at the AC layer surface was greater than that of the AC layer bottom on the entire wheel load. The shear stress was the highest at the wheel load center of both the AC layer surface and bottom, reaching 0.125 MPa and 0.313 MPa, respectively.

For transverse stress, under the introduced temperature field, the entire AC layer was subjected to tensile stresses. The vehicle load action may have instead reduced the magnitude of the tensile stress, so the transverse tensile stress at the wheel load center was lower. For longitudinal stress, for the same reason as for the transverse stress, the entire AC layer was subjected to tensile stresses. Since the wheel load was a partial load, a small misalignment of the cracks in the CRC layer occurred. This small misalignment may have resulted in the longitudinal compressive stress at the bottom of the asphalt layer in contact with the CRC layer crack and the longitudinal tensile stress at the AC layer surface. The coupling of the partial load and temperature load resulted in low longitudinal tensile stress at the bottom of the asphalt layer and high longitudinal tensile stress at the surface. For shear stress, the small misalignment in the surface and the bottom of the AC layer generated high shear stress at the center of the wheel load.

These results demonstrate that longitudinal cracks were more likely to generate on the wheel load side and the wheel load gap with channelized traffic, and the wheel load center tended to incur more top-down transverse cracks. What is more, the shear stress might have aggravated the development of cracks, especially the higher shear stress at the bottom of the AC layer. In fact, the asphalt layer section is not always in the same position as the wheel load. For example, the section was at the wheel load gap this time, but it might be at the wheel load center. In this case, the asphalt layer bottom and layer surface were alternately subjected to greater tensile and shear stress. As a result, there was a high probability that cracks developed from both the bottom and surface of the AC layer, i.e., “corresponding cracks”.

3.1.2. Unfavorable Driving

Considering the high shear stress and higher tensile stress in the AC layer during turning and emergency braking, the distribution of the shear stress and the longitudinal and transverse tensile stress of the AC layer during turning and emergency braking was analyzed. The distribution of the shear stress is illustrated in Figure 7a–c.

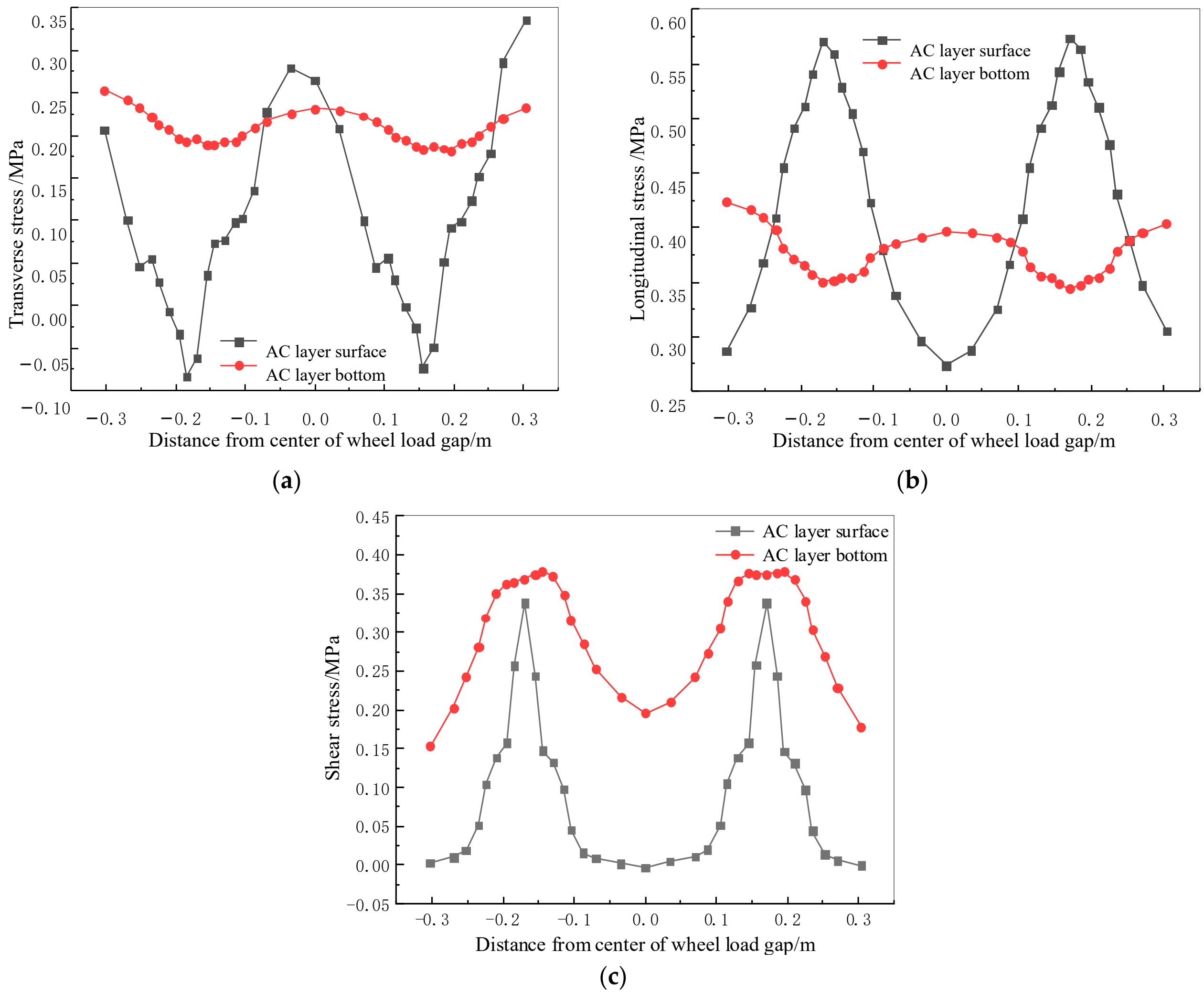

Figure 7. Stress of AC layer under unfavorable conditions: (**a**) distribution of transverse stress; (**b**) distribution of longitudinal stress; (**c**) distribution of shear stress.

Figure 7 demonstrates that the stress distribution regularity of the AC layer under unfavorable driving conditions was almost the same as under normal driving conditions except for the longitudinal stress. According to Figure 7a, the maximum transverse tensile stress appeared on the right side of the wheel load, rather than near the wheel load gap. The maximum transverse tensile stress was 0.336 MPa, an increase of 29.7% compared to normal driving. It can be seen in Figure 7b that the distribution regularity of the longitudinal stress under unfavorable driving was almost the same as that under normal driving; the difference was in the wheel load gap, where the longitudinal stress of the AC layer bottom was greater than that of the AC layer surface. The maximum longitudinal tensile stress wheel load center of the AC layer was 0.573 MPa, which increased by 76.9% under unfavorable driving. As shown in Figure 7c, the maximum shear stress on both the AC layer surface and bottom appeared at the wheel load center, reaching 0.338 MPa and 0.379 MPa, respectively. At the same time, the shear stress values increased by 170.4% and 21.1%, respectively.

The changes in the location and maximum stress value distributions were due to the fact that both the direction and magnitude of the force enacted on the road surface by the wheel load changed under the effect of turning and braking. The transverse force was transformed from originally existing only inside the wheel load area of action to the overall direction opposite to the direction of the turning. The longitudinal force was increased due to the effort of braking, resulting in the increase in the tensile and shear stress.

In conclusion, when cars emergency braked on the curve, the stress increased to varying degrees, especially the surface longitudinal tensile stress and the surface shear stress. The transverse stress on the inside of the curve under unfavorable driving was also greater than that under normal driving. So, longitudinal cracks were more likely to generate inside of the curve. Emergency braking on the curve usually happens on curves with poor stadia. Thus, transverse cracks occurred more easily on the poor stadia curves. To prevent or relieve such problems, it is necessary to improve the crack resistance of the CRC layer, or a crack-resistant interlayer should be set, and asphalt mixtures with better crack resistance in the AC layer should be used.

3.2. Analysis of Asphalt Layer Thickness Influence on Mechanical Behavior

The CRC + AC composite pavement model and parameters were kept constant, except for the thickness of the AC layer. In order to investigate the influence of the AC layer thickness on mechanical performance, the thickness of the AC layer was changed from 4 cm to 14 cm. The maximum stress variations with the AC layer thickness are shown in Figure 8a–d.

From Figure 8a,b, it can be seen that the maximum longitudinal and transverse tensile stress on the surface and bottom of the AC layer decreased with the increase in the AC layer thickness. As the thickness of the AC layer increased from 4 cm to 14 cm, the AC layer surface stress decreased slightly, but the AC layer bottom stress decreased sharply. The transverse stress on the surface decreased by 0.061 MPa, and the longitudinal stress decreased by 0.014 MPa. The transverse stress at the bottom of the AC layer decreased by 0.546 MPa and the longitudinal stress decreased by 0.312 MPa. Changes in the thickness of the AC layer had little effect on the surface shear stress, as shown in Figure 8c,d. As the thickness of the AC layer increased from 4 cm to 14 cm, the surface shear stress decreased slightly, but the bottom shear stress of the AC layer near the micro-cracks of the CRC layer decreased dramatically, by about 60%.

The reasons for the decrease in stress may be as follows. On the one hand, the increased AC layer thickness decreased the temperature gradient in the pavement structure, and the tensile stress was reduced due to the temperature effect. On the other hand, the increased AC layer thickness increased the degree of stress dispersion. So, the stresses acting upon the cracks of the CRC layer were reduced. The stress concentration at the bottom of the AC layer caused by the small misalignment of the cracks was also lower, and the stress in the asphalt layer was similarly reduced.

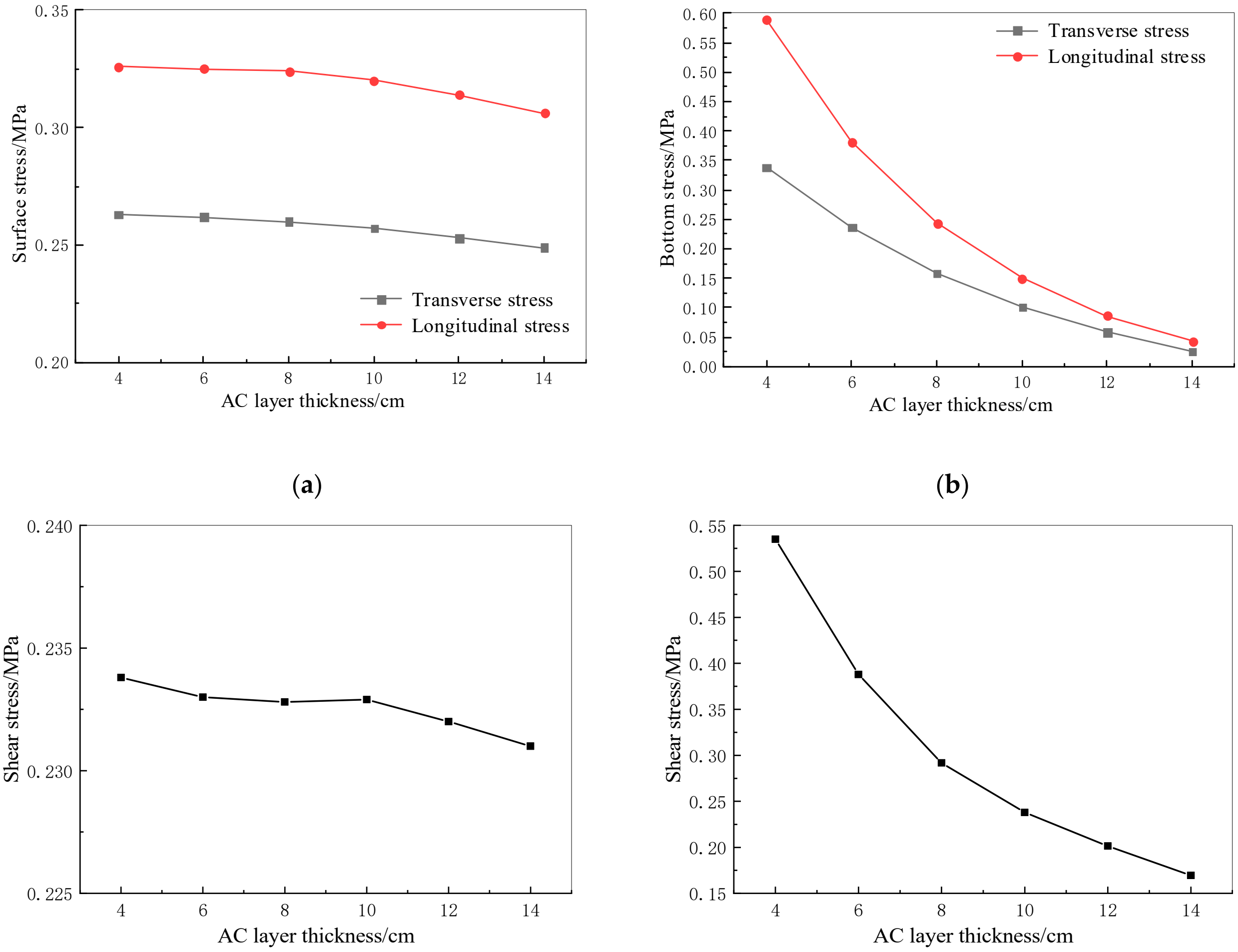

(**a**) (**b**)

(**c**) (**d**)

Figure 8. Effects of AC layer thickness on stress: (**a**) effect on tensile stress of the AC layer surface; (**b**) effect on tensile stress of the AC layer bottom; (**c**) effect on shear stress of the AC layer surface; (**d**) effect on shear stress of the AC layer bottom.

In summary, it is obvious that the thickness had a greater impact on the AC layer bottom stress than on the AC layer surface, and the influence on the longitudinal stress was greater than that on the transverse stress. This might indicate that pavement diseases, such as slippage induced by excessive shear stress at the interlayer interface, as well as early damage, such as reflection fractures caused by the stress concentration, could be reduced by controlling the thickness of the AC layer. If the proposed asphalt layer is thin, an asphalt mixture with good crack and shear resistance should be chosen, and crack resistance measures should be adopted in the engineering design at the interface between layers.

3.3. Reasonable AC Layer Thickness Analysis

Due to the thinness of the AC layer and the large difference in the modulus between the AC and CRC layers, the asphalt layer was more likely to be penetrated by cracks. The thickness of the asphalt layer has a great influence on the rate of crack expansion [20,21]. Therefore, the thickness design of a rigid–flexible composite pavement asphalt layer is important. According to the literature [25], asphalt layer cracking is more influenced by tensile and shear stresses. So, it was necessary to study the shear stress at different depths of the AC layer and its variation with different thicknesses. The results are shown in Figure 9.

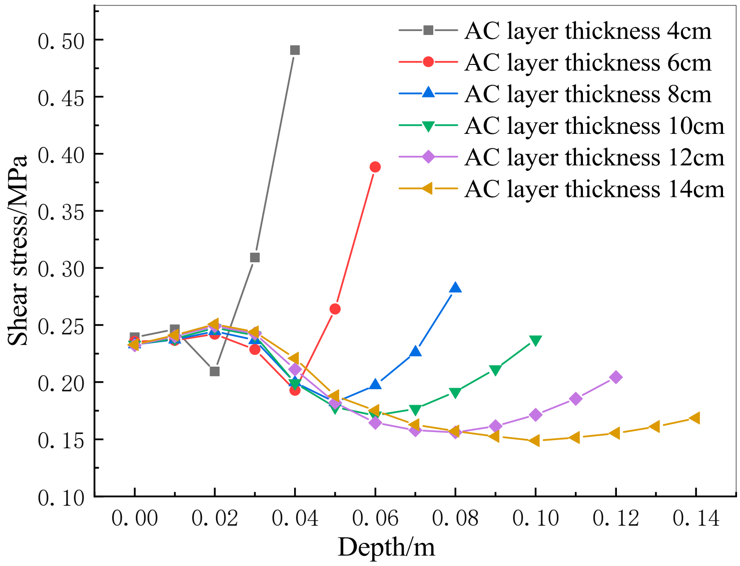

Figure 9. Shear stress changes at different depths with AC layer thickness.

Figure 9 shows that the shear stress at the bottom and 2 cm~3 cm deep in the AC layer was higher when the AC layer thickness was 4 cm~8 cm, and the shear stress at the bottom was greater. The maximum shear stress at the AC layer bottom was 1.9 times that inside the AC layer when the thickness of the AC layer was 4 cm, and it was 1.2 times lower when the thickness was 8cm. The maximum shear stress at the AC layer bottom decreased gradually with the increase in thickness. When the AC thickness was 10 cm, the maximum shear stress inside the AC layer and at the AC layer bottom was basically the same. The maximum shear stress at the AC layer bottom was 0.8 times that inside the AC layer when the thickness of the AC layer was 12 cm, and it was 0.68 times lower when the thickness of the AC layer was 14 cm. The decrease in the sheer stress at the AC layer bottom also occurred because of the previously mentioned stress dispersion.

The maximum longitudinal tensile stress and shear stress at the AC layer bottom were higher. Changes in the maximum tensile stress and shear stress at the AC layer bottom occurred when the AC thickness increased from 4 cm to 14 cm, as shown in Table 6.

Table 6. Influence of AC layer thickness change on the tensile and shear stress at bottom.

Thickness Increment/cm	Longitudinal Stress Reduction/%	Shear Stress Reduction/%
4 to 6	−35.31	−27.20
6 to 8	−36.22	−24.87
8 to 10	−21.00	−13.86
10 to 12	−17.59	−9.43
12 to 14	−12.60	−8.18

According to Table 6, the reduction rate of the longitudinal tensile stress and shear stress decreased with the increase in the AC layer thickness. For example, when the AC layer thickness increased from 4 cm to 6 cm, the maximum longitudinal tensile stress decreased by 35.31%, and maximum shear stress decreased by 27.2%. These reductions were larger when the AC layer thickness was below 8 cm; however, when the AC layer thickness increased from 8 cm to 10 cm, the maximum longitudinal tensile stress decreased by 21.00% and the maximum shear stress decreased by 13.86%. The reduction decreased and the decreasing trend intensified with the increase in the AC layer thickness. The reason for this phenomenon may be because, as the thickness of the AC layer increased, the diffusion of stress at the AC layer bottom decreased, resulting in a reduction of the effect of increasing thickness on stress reduction. The reduction rate varied considerably when the AC layer was 8 cm thick. Considering the economy of engineering, the recommended thickness of the asphalt layer is 8 cm~12 cm. These results are similar to those found in the studies by Fardin and Santos [18] and Fang et al. [29].

3.4. Physical Engineering AC Layer Cracking Analysis

The physical engineering under investigation was a section of the Beijing–Hong Kong–Macao National Expressway (G4) in Hunan, which has a high traffic flow and many overweight vehicles and is a CRC + AC composite pavement structure based on the upgrading of old cement pavement. The pavement structure is shown in Table 7.

Table 7. Combination and thickness of pavement structure layer of physical engineering.

Structure Layer	Structural Material and Thickness
Surface layer	4 cmSBS modified asphalt SMA13
Bonding layer	0.3 L·(m^2)$^{-1}$~0.6 L·(m^2)$^{-1}$ modified emulsified asphalt
Subsurface	6 cm SBS modified asphalt AC-20
Bonded waterproof anti-cracking layer	Impregnation 1.40 kg·(m^3)$^{-1}$ heavy traffic asphalt (A-70) polyester filament burnt geotextiles
Reinforced layer, leveling layer	18 cm CRC
Isolation layer	2.5 cm asphalt mixture AC-10I
Binding layer	0.3 L·(m^2)$^{-1}$~0.5 L·(m^2)$^{-1}$ emulsified asphalt or 0.3 kg·(m^2)$^{-1}$~0.6 kg·(m^2)$^{-1}$ heavy traffic asphalt A-70
Former concrete layer	Slab replacement slurry treatment of old concrete slabs

The rut depth of CRC + AC composite pavement is small, and the main disease is asphalt layer cracking, according to the above physical engineering's tracking observation and core sampling. The samples are shown in Figure 10; (a) is the sample of "corresponding cracks", and (b) is the sample of reflection cracks.

(**a**) (**b**)

Figure 10. Three-dimensional non-uniform load (size unit: cm): (**a**) Normal driving; (**b**) unfavorable driving.

From the samples and survey results, asphalt layer cracking was mainly reflected in two categories: One was the top-down cracks in AC mainly caused by the effects of tensile and shear stress and temperature changes and which generally extended only about 2 cm down from the surface to the bottom. They mainly manifested as longitudinal cracks near the wheel path zone, a small number of transverse cracks, and "U" type slippage cracking on the surface of the climbing section. The other category was due to the existence of transverse random micro-cracks in the CRC layer itself, which caused the stress concentration effect at the AC layer bottom and the contraction of the CRC micro-cracks, resulting in the cracking of the AC layer bottom under high tensile and shear stress. In addition, to control cracking, the current design method in China is to control the average width of CRC cracks, which means that the crack width of some micro-cracks in the CRC layer might be rather large. This is also one of the reasons for the damage and cracking at the AC layer bottom. Together with the transverse top-down cracks, the "corresponding cracks" (cracking from both the surface and bottom side) may cause slippage and cracking between the asphalt layer and the CRC layer when the cracks expand.

Overall, the simulation results of the mechanical behavior of the CRC + AC composite pavement asphalt layer are in good agreement with the physical engineering investigation and observation results. They can provide a theoretical and scientific basis for cracking control and the reasonable design of a CRC + AC composite pavement asphalt layer.

4. Conclusions

The mechanical behavior, cracking characteristics, and mechanism of a CRC + AC composite pavement asphalt layer were revealed by thermal–mechanical coupling simulation analysis and the investigation and tracking observation of physical engineering. Control measures were put forward, and the main conclusions are as follows:

1. Under normal driving conditions, the AC layer, which is usually in the position of the wheel load gap and wheel load side, more easily incurs longitudinal cracks. In the actual situation, the asphalt layer bottom and layer surface are alternately subjected to greater tensile and shear stresses, which may cause transverse "corresponding cracks".
2. Under unfavorable driving, longitudinal cracks are more likely to generate inside of the curve. Due to emergency braking on curves, they usually occur on curves with poor stadia. So, it is also easier for transverse cracks to occur on poor stadia curves under normal driving.
3. The AC layer is more prone to bottom-up cracking when its thickness is less than 8 cm, and it is more prone to top-down cracking when its thickness is more than 8 cm. Comprehensively considering the tensile and shear stress and the thickness of the asphalt layer, it is recommended that the suitable thickness range of the AC layer is 8 cm~14 cm.
4. The physical engineering investigation and observation results are in good agreement with the analyzed mechanical behavior and the predicted crack formations of the CRC + AC composite pavement asphalt layer. This indicates that the results of the study are helpful for the design of AC layer thickness and cracking prevention strategies for CRC + AC composite pavements.

Author Contributions: Conceptualization, S.L. and S.Y.; methodology, Y.S., L.X. and X.L.; validation, Y.S. and J.Y.; investigation, S.L.; resources, X.L.; data curation, J.Y.; writing—original draft preparation, Y.S. and L.X.; writing—review and editing, Y.S.; visualization, Y.S.; supervision, S.L. and S.Y.; project administration, L.X.; funding acquisition, S.L. All authors have read and agreed to the published version of the manuscript.

Funding: This research was funded by The National Key Research and Development Program of China (Grant No. 2021YFB2601000), the National Natural Science Foundation of China (Grant No. 51878076), and the National Science Foundation of Hunan Province, China (Grant No. 2022JJ30598).

Institutional Review Board Statement: Not applicable.

Informed Consent Statement: Not applicable.

Data Availability Statement: The data used to support the findings of this study are available from the corresponding author upon request.

Conflicts of Interest: The authors declare that they have no conflict of interest, no competing financial interests, and no personal relationships that could have appeared to influence the work reported in this paper.

References

1. Ren, D.; Song, H.; Huang, C.; Xiao, C.; Ai, C. Comparative evaluation of asphalt pavement dynamic response with different bases under moving vehicular loading. *J. Test. Eval.* **2019**, *48*, 1823–1836. [CrossRef]
2. Liu, X.; Zhang, X. Asphalt pavement dynamic response under different vehicular speeds and pavement roughness. *Road Mater. Pavement Des.* **2019**, *22*, 1287–1308. [CrossRef]
3. Shen, K.; Zhang, H.; Tong, J.; Wang, H.; Chen, X. Dynamic elastic analysis of flexible pavements under moving vehicles: A semi-analytical finite element treatment. *Road Mater. Pavement Des.* **2021**, *23*, 1440–1450. [CrossRef]
4. Ban, H.; Im, S.; Kim, Y.-R.; Jung, J.S. Laboratory tests and finite element simulations to model thermally induced reflective cracking of composite pavements. *Int. J. Pavement Eng.* **2017**, *19*, 220–230. [CrossRef]
5. Ling, M.; Chen, Y.; Hu, S.; Luo, X.; Lytton, R.L. Enhanced model for thermally induced transverse cracking of asphalt pavements. *Constr. Build. Mater.* **2019**, *206*, 130–139. [CrossRef]
6. Peng, Y.; Xia, S.; Xu, Y.-R.; Lu, X.-Y.; Li, Y.-W. Mechanical Response of Asphalt Surfaces under Moving Traffic Loads Using 3D Discrete Element Method. *J. Transp. Eng. Part B Pavements* **2022**, *148*, 04022006. [CrossRef]
7. Chen, E.; Zhang, X. Dynamic Analysis of Viscoelastic Asphalt Pavement under Vehicle–Bridge Interaction Load. *J. Transp. Eng. Part B Pavements* **2021**, *147*, 04021050. [CrossRef]
8. Lu, G.; Wang, C.; Liu, P.; Pyrek, S.; Oeser, M.; Leischner, S. Comparison of Mechanical Responses of Asphalt Mixtures under Uniform and Non-Uniform Loads Using Microscale Finite Element Simulation. *Materials* **2019**, *12*, 3058. [CrossRef]
9. Baek, C.M. Investigation of Top-Down Cracking Mechanisms Using the Viscoelastic Continuum Damage Finite Element Program. Ph.D. Thesis, North Carolina State University, Raleigh, North Carolina, 2010.
10. Ziari, H.; Aliha, M.R.M.; Mojaradi, B.; Jebalbarezi Sarbijan, M. Investigating the effects of loading, mechanical properties and layers geometry on fatigue life of asphalt pavements. *Fatigue Fract. Eng. Mater. Struct.* **2019**, *42*, 1563–1577. [CrossRef]
11. Islam, M.R.; Tarefder, R.A. Contribution of Day-Night Temperature Fluctuation to Top-Down Cracking in Asphalt Pavement. *J. Cold Reg. Eng.* **2018**, *32*, 06017006. [CrossRef]
12. Wu, S.; Muhunthan, B. A mechanistic-empirical model for predicting top-down fatigue cracking in an asphalt pavement overlay. *Road Mater. Pavement Des.* **2018**, *20*, 1322–1353. [CrossRef]
13. Aliha, M.R.M.; Ziari, H.; Sobhani Fard, E.; Jebalbarezi Sarbijan, M. Heterogeneity effect on fracture parameters of a multilayer asphalt pavement structure containing a top-down crack and subjected to moving traffic loading. *Fatigue Fract. Eng. Mater. Struct.* **2021**, *44*, 1349–1371. [CrossRef]
14. Rith, M.; Kim, Y.K.; Lee, S.W. Reflective cracking from thermal loading in asphalt–concrete composite pavements. *Proc. Inst. Civ. Eng.-Transp.* **2022**, *175*, 178–186. [CrossRef]
15. Tajdini, M.; Taherkhani, A. Investigating the performance of cracked asphalt pavement using Finite Elements Analysis. *Civ. Eng. Infrastruct. J.* **2020**, *53*, 33–51.
16. Zhao, Y.; Alae, M.; Fu, G. Investigation of mechanisms of top-down fatigue cracking of asphalt pavement. *Road Mater. Pavement Des.* **2017**, *19*, 1436–1447. [CrossRef]
17. Shabbir Hossain, M.; Nair, H.; Celik Ozyildirim, H. Construction of a Composite Pavement (Asphalt over Concrete) in Virginia. *Transp. Res. Rec.* **2022**, *1*, 03611981221089300. [CrossRef]
18. Fardin, H.E.; Santos, A.G.d. Predicted responses of fatigue cracking and rutting on Roller Compacted Concrete base composite pavements. *Constr. Build. Mater.* **2021**, *272*, 121847. [CrossRef]
19. Xie, P.; Wang, H. Analysis of Temperature Variation and Thermally-Induced Reflective Cracking Potential in Composite Pavements. *Transp. Res. Rec. J. Transp. Res. Board* **2020**, *2674*, 177–188. [CrossRef]
20. Alae, M.; Haghshenas, H.F.; Zhao, Y. Evaluation of top-down crack propagation in asphalt pavement under dual tires loading. *Can. J. Civ. Eng.* **2019**, *46*, 704–711. [CrossRef]
21. Diallo, A.O.; Akpinar, M.V. Mechanistic Responses of Asphalt Concrete Overlay Over Jointed Plain Concrete Pavement Using Finite Element Method. *Balt. J. Road Bridge Eng.* **2020**, *15*, 80–93. [CrossRef]
22. Li, S.; Li, Y.; Liu, Z.; Sun, Z.J. Interlaminar Shear Stress and Structure of Continuously Reinforced Concrete Composite Asphalt Pavements. *J. Highw. Transp. Res. Dev.* **2012**, *7*, 9–16. [CrossRef]
23. Li, S.; Liu, Z. *Theory and Technology of Durability of Rigid-Flexible Composite Pavement*; China Communications Press: Beijing, China, 2014.
24. Zhao, X.; Shen, A.; Ma, B. Temperature response of asphalt pavement to low temperatures and large temperature differences. *Int. J. Pavement Eng.* **2018**, *21*, 49–62. [CrossRef]
25. Alae, M.; Ling, M.; Haghshenas, H.F.; Zhao, Y. Three-dimensional finite element analysis of top-down crack propagation in asphalt pavements. *Eng. Fract. Mech.* **2021**, *248*, 107736. [CrossRef]
26. Liu, Z.; Liu, Y.; Gao, Q. In-plane flexible ring modeling and a nonlinear stiffness solution for heavy-load radial tires. *Mech. Syst. Signal Process.* **2022**, *171*, 108956. [CrossRef]
27. Liu, Y.; Qian, Z.; Liu, C.; Huang, Q. Investigation on Hydroplaning Behaviors of a Patterned Tire on a Steel Bridge Deck Pavement. *Appl. Sci.* **2021**, *11*, 10566. [CrossRef]
28. Zhang, Z.; Fu, H.; Liang, X.; Chen, X.; Tan, D. Comparative Analysis of Static and Dynamic Performance of Nonpneumatic Tire with Flexible Spoke Structure. *Stroj. Vestn.—J. Mech. Eng.* **2020**, *66*, 458–466. [CrossRef]
29. Fang, N.; Li, H.; Li, Q.; Wang, X.; Hu, S.; Xin, L. Study on asphalt layer of composite pavement temperature shrinkage stress considering stress relaxation. *Mater. Struct.* **2021**, *54*, 32. [CrossRef]